Calculation and Experimental Test of the Cooling Factor of Tungsten

T Pütterich[1], R Neu[1], R Dux[1], A D Whiteford[2], M G O'Mullane[2], H P Summers[2] and the ASDEX Upgrade Team[1]

[1] *Max-Planck-Institut für Plasmaphysik, EURATOM Association, D-85748 Garching, Germany*

[2] *Department of Physics, University of Strathclyde, Glasgow G4 0NG, UK*

Abstract. The cooling factor of W is evaluated using state of the art data for line radiation and an ionization balance which has been benchmarked with experiment. For the calculation of line radiation, level-resolved calculations were performed with the Cowan code to obtain the electronic structure and excitation cross sections (plane-wave Born approximation). The data were processed by a collisional radiative model to obtain electron density dependent emissions. These data were then combined with the radiative power derived from recombination rates and Bremsstrahlung to obtain the total cooling factor. The effect of uncertainties in the recombination rates on the cooling factor were studied and were identified to be of secondary importance. The new cooling factor is benchmarked, by comparisons of the line radiation to spectral measurements as well as to a direct measurement of the cooling factor. Additionally, a less detailed calculation using a configuration averaged model was performed. It was used to benchmark the level-resolved calculations and to improve the prediction on radiation power from line radiation for ionization stages which are computationally challenging. The obtained values for the cooling factor validate older predictions from literature. Its ingredients and the absolute value are consistent with the existing experimental results regarding the value itself, the spectral distibution of emissions and the ionization equilibrium. A table of the cooling factor versus electron temperature is provided. Finally, the cooling factor is used to investigate the operational window of a fusion reactor with W as intrinsic impurity. The minimum value of $nT\tau_E$, for which a thermonuclear burn is possible, is increased by 20% for a W concentration of $3.0 \cdot 10^{-5}$ compared to a plasma without any impurities, except for the He ash which is considered in both cases.

PACS numbers: 28.52, 32.30, 34.80, 52.20, 52.25, 52.40, 52.55

Nuclear Fusion Thomas.Puetterich@ipp.mpg.de

1. Introduction

Tungsten (W) is well suited as a plasma facing component (PFC) in terms of power handling capability, low erosion yield and low deuterium retention [1, 2]. However, when the W concentration exceeds a certian level in the central part of the plasma the radiative losses limit the plasma operation and performance such that for ITER the central concentration lower than several 10^{-5} is obligatory [3]. This has been found earlier in the ORMAK [4] and PLT [5] tokamaks in which the central W radiation prevented fusion relevant plasma operation due to W concentrations in the range of 10^{-3}. Due to the use of a divertor and other operational precautions the W concentration can be controlled to low enough values [6] and fusion relevant operation is possible as demonstrated at ASDEX Upgrade [7, 8]. Still, the radiative cooling by W is a concern and the maximum tolerable W concentration

is an important value for ITER and a future fusion reactor. This value, however, is based on calculations of the cooling factor [9, 10] using the average ion model, a model which does not calculate quantummechanical wave functions of the levels in each ion, but uses scale formulas based on a hydrogenic orbital model. In this work, the Cowan code [11] is used for level resolved calculations in order to calculate a cooling factor based on more detailed atomic physics. Such atomic data allow for spectroscopic comparisons in which the spectral contributions to the cooling factor can be benchmarked. The data calculations in this work underwent such a benchmark with experimental spectra, which underlines their credibility. Due to the fact, that the level resolved calculations of cross sections for electron impact excitation are too large and time consuming for ionization states below about Cd-like W^{26+} the calculations have been supported and extended using a configuration averaged model, which allowed to tackle all ionization states of W. It may be noted that a detailed work on the interplay between configuration averaged and level-resolved calculations for high-Z elements can be found in [12].

2. Atomic Data

2.1. Ionization Equilibrium

In [13], a detailed analysis of the ionization equilibrium has been performed which compared measured results for Pd-like W^{27+} to Fe-like W^{48+} to the predictions derived from different combinations of ionization and recombination rates. The best agreement has been found for a set of ionization rates, which originate from configuration averaged distorted wave (CADW) calculations [14] and recombination rates which originate from the average ion model [9] but have been adjusted by temperature independent factors to match the experimental observations. These adjustments have been performed ad-hoc without a physics explanation to provide a set of ionization and recombination rates that led to an ionization equilibrium as observed in experiment. These adjustments are used also in the present work. In order to check the influence of the ionization equilibrium,a sensitivity study is presented in section 2.5. It should be noted that the ionization rates are evaluated for zero density while the optimization of the ionization equilibrium has been performed in the density range $5 - 10 \cdot 10^{19}\,\mathrm{m}^{-3}$. Due to the fact that the ionization rates are expected to vary weakly in the reactor relevant density range the ionization balance obtained in [13] is relevant for this range. Concerning the recombination rates, it should be noted that there are rates of higher quality for a few ionization stages (e.g. DR rates of Ni-like W [15], Ar-like W [16] and Ne-like W [17]) available. However, for a compilation of the cooling factor, rates for all ions are needed. A comparison of the rates used in this work to the mentioned rates of higher quality gives agreement within a factor of 2 in the relevant electron temperature ranges.

2.2. Radiation due to Recombination and Bremstrahlung

To provide a consistent set of radiation power with respect to the adjusted recombination rates a rather simple model is chosen to calculate the radiation emitted during the recombination process. When an electron is captured by an ion the radiation energy which is emitted during the recombination and the following cascade equals the ionization potential plus the kinetic energy of the electron minus the kinetic energy gain of the recombined ion. Due to the large difference of ion and electron mass the kinetic energy gain of the recombined ion can be neglected. For simple radiative recombination the involved electron energies are comparably small, while only for dielectronic recombination electron energies up to a

maximum of two times the ionization potential play a major role. In the following the radiation emitted during recombination is approximated by $f_{rec-rad}$ times the ionization potential times the recombination rate. As small electron energies are most important for the recombination rates, $f_{rec-rad} = 1.2$ is used. For this approximation, an uncertainty of less than 20% is anticipated because it includes the lower limit for $f_{rec-rad}$. However, values of $f_{rec-rad} > 1.4$ are possible. Therefore, the impact of the value of $f_{rec-rad}$ on the cooling factor is investigated separately in section 2.5. For the major part of the electron temperature range under consideration this contribution to the total cooling factor is small. The contribution of Bremstrahlung is calculated using the formula of [9] and the free-free Gaunt factor of [18].

2.3. Line Radiation

In the following two types of calculations, i.e. the level-resoved (LR) and configuration averaged (CA) calculations, are varied and compared. The LR calculation treats each level separately which results in large computations. For certain ionization stages (e.g. stages with open f- or d-orbitals), the computational effort is so large that either the calculation could not be performed (e.g. below Cd-like W^{26+}) or the computational effort had to be decreased by allowing for less wave functions (i.e. including less configurations in the calculations) possibly neglecting contributions to the radiated power. In that case the important spectral features might be predicted as observed and benchmarked in [13], but less obvious spectral features could make up this missing power. The CA calculation does not include the details of each level and is less accurate concerning the spectral distribution of radiation. It might also show inaccuracies in the total radiated line power as to some extent the detailed physics of the levels could be important. However, large sets of configurations can be included in the calculations which is the strength of the CA calculations and which allows to tackle the charge stages below Cd-like W^{26+}. In the following, there will be references to one LR calculation and two CA calculations (i.e. CA-LR and CA-LARGE). The CA-LR calculation includes for each charge stage the same sets of configurations as the LR calculation. A comparison thus allows to identify differences which occur due to the type of calculations. The CA-LARGE calculation includes a very large set of configurations and a comparison between CA-LR and CA-LARGE gives information about the missing radiation due to the smaller set of configurations used in the LR and CA-LR calculation.

The elaborate LR calculations (cf. [13]) and the CA calculations for each W ion have been performed using the Cowan code via the front end and infrastructure provided by the ADAS project [19]. The calculations determined the electronic structure including transition probabilities and the cross sections for electron impact excitation. Electric and magnetic dipole and electric quadrupole transitions have been included in the calculation using the plane-wave Born approximation for the excitation part. A collisional-radiative modelling was then applied to determine the spectra of each ionization stage separately. In the following a density of $7.5 \cdot 10^{19}\,\mathrm{m}^{-3}$ is chosen for all presented plots. A variation in density in the range $5 - 15 \cdot 10^{19}\,\mathrm{m}^{-3}$ has been performed, but does not change the results significantly. This work follows detailed investigations (cf. [13]) about the dominant spectral features emitted by W. In the course of these investigations the ionization balance was adjusted to the experimental findings and LR calulations have been compared to measured spectra and their dependence on electron temperatures (cf. also [20]). In table 1, the input configurations for five ionization stages and calculation methods are given. In figure 1, the corresponding results on the emissivity coefficient for line radiation C_{line} is given. The power density P_q for line radiation from a single ionization stage q with density n_q is given by $P_q = n_e \cdot n_q \cdot C_{line}$.

The difference between the three calculation methods (LR, CA-LR, CA-LARGE) varies

	LR/CA-LR	CA-LARGE
Mo-like W^{32+}	$4d^6$, $4d^5 4f \rightarrow 4d^5\,5f$, $4p^5\,4d^7$, $\Sigma = 7$	$4d^6$, $4d^5 4f \rightarrow 4d^5 5g$, $4p^5 4d^7 \rightarrow 4p^5 4d^6 5g$, $4s4p^6 4d^7 \rightarrow 4s4p^6 4d^6 5g$, $3d^9 4s^2 4p^6 4d^7 \rightarrow 3d^9 4s^2 4p^6 4d^6 5g$; $\Sigma = 28$
Rb-like W^{37+}	$4p^6 4d \rightarrow 4p^6 5f$, $4p^5 4d^2 \rightarrow 4p^5 4d5f$, $4s4p^6 4d^2 \rightarrow 4s4p^6 4d5f$, $\Sigma = 18$	$4p^6 4d \rightarrow 4p^6 5g$, $4p^5 4d^2 \rightarrow 4p^5 4d5g$, $4s4p^6 4d^2 \rightarrow 4s4p^6 4d5g$, $3d^9 4s^2 4p^6 4d^2 \rightarrow 3d^9 4s^2 4p^6 4d5g$; $\Sigma = 28$
Kr-like W^{38+} (no difference)	$4p^6$,$4p^5 4d \rightarrow 4p^5 5g$, $4s4p^6 4d \rightarrow 4s4p^6 5g$, $3d^9 4s^2 4p^6 4d \rightarrow 3d^9 4s^2 4p^6 5g$, $\Sigma = 22$	$4p^6$,$4p^5 4d \rightarrow 4p^5 5g$, $4s4p^6 4d \rightarrow 4s4p^6 5g$, $3d^9 4s^2 4p^6 4d \rightarrow 3d^9 4s^2 4p^6 5g$, $\Sigma = 22$
Ni-like W^{46+} (no difference)	$3d^{10}$, $3d^9 4s \rightarrow 3d^9 5g$, $3p^5 3d^{10} 4s \rightarrow 3p^5 3d^{10} 5g$, $3s3p^6 3d^{10} 4s \rightarrow 3s3p^6 3d^{10} 5g$, $\Sigma = 28$	$3d^{10}$, $3d^9 4s \rightarrow 3d^9 5g$, $3p^5 3d^{10} 4s \rightarrow 3p^5 3d^{10} 5g$, $3s3p^6 3d^{10} 4s \rightarrow 3s3p^6 3d^{10} 5g$, $\Sigma = 28$
Ti-like W^{52+}	$3d^4$, $3d^3 4s \rightarrow 3d^3 4f$ $3p^5\,3d^5$, $\Sigma = 6$	$3d^4$, $3d^3 4s \rightarrow 3d^3 5g$, $3p^5 3d^5 \rightarrow 3p^5 3d^4 5g$, $3s3p^6 3d^5 \rightarrow 3s3p^6 3d^4 5g$; $\Sigma = 30$

Table 1. Used input configurations for the level-resolved (LR) (cf. [13]) and corresponding configuration averaged (CA-LR) calculation and the extended configuration averaged (CA-LARGE) calculation. The arrow in between two configurations indicates that all configurations were included which result from a stepwise propagation of the outermost electron (e.g. $4s^2 \rightarrow 4s4d$ means $4s^2$, 4s4p, 4s4d).

with the complexity of the targeted ionization stage. For Mo-like W^{32+} the level-resolved calculation allowed to include only the seven most important configurations (open 4d-shell), such that the experimentally observed, intense spectral feature around 5 nm is reproduced (cf. [13]). When comparing C_{line} from the LR-calculation to that from the CA-LR calculation in figure 1(a) a rather good agreement is found, which validates the configuration averaged approach. Even the shape of the two C_{line} graphs versus T_e matches well, although the individual energy levels which yield thresholds for the single electron impact excitations are not resolved in the CA calculation. Further emissions in the spectra are not experimentally attributed to this ionization stage, however, it is clear that an inclusion of higher excited configurations is connected to additional emissions. This inclusion is performed by the CA-LARGE calculation, which consequently arrives at larger C_{line} values as is presented in figure 1(a). The results for Ti-like W^{52+} (cf. figure 1(a)) resembles the features for the Mo-like W^{32+}. As the LR calculation must already take 770 levels into account (open 3d-shell) an extension of the input configurations is not easily possible. For Rb-like W^{37+} (cf. figure 1(c)), already the LR and CA-LR calculations are large enough to include most of the emissions which are calculated by the CA-LARGE calculation. Similarly, the results for Ni-like W^{46+} (cf. figure 1(b)) arrive at a very good agreement between LR and CA-LR, while the set of configurations used in the LR calculation is already very large and was not extended in the CA-LARGE calculation. It was possible to choose the set of configurations for the LR calculation so large because the ground state exhibits a closed subshell which translates

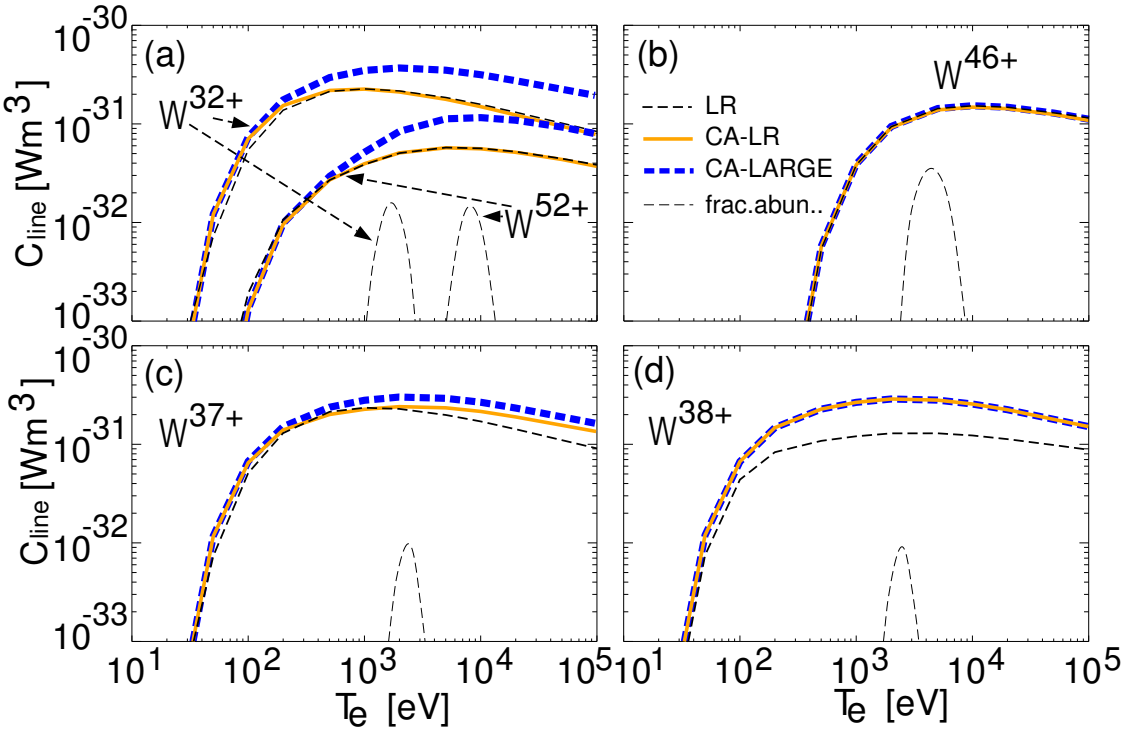

Figure 1. (colored in online-version) (a) Emissivity coefficient for line radiation C_{line} arising from different calculation procedures (i.e. level-resolved (LR), configuration averaged with LR configuration set (CA-LR) and configuration averaged with large configuration set (CA-LARGE)) and fractional abundances multiplied by 10^{-31} Wm^3 (to fit into plot) for Mo-like W^{32+} and Ti-like W^{52+}. (b) sames as (a) for Ni-like W^{46+}; (c) sames as (a) for Rb-like W^{37+}; (d) sames as (a) for Kr-like W^{38+}.

in a much smaller number of levels for ground configuration (one level) and the excited configurations and thus less computational effort. For a few cases like for Kr-like W^{38+} (cf. figure 1(d)) a discrepancy is observed already between the LR and CA-LR calculation. This effect will be discussed below. In figure 2 the three calculation procedures are compared for the ionization stages from Ag-like W^{28+} to He-like W^{72+}. The C_{line} graphs for each ionization stage are evaluated at the electron temperature at which the fractional abundance of the respective ionization stage reaches its maximum. Two systematic behaviours get apparent. For ionization stages exhibiting a ground state with more than two and less than eight electrons in a d-shell the LR calculation agrees with the CA-LR calculation, while the CA-LARGE calculation predicts more radiation. The second observation is that for the ionization stages Ag-like W^{28+}, Kr-like W^{38+} and Ar-like W^{56+} discrepancies get apparent between the LR and CA-LR calculations while the CA-LARGE agrees with the latter. The first observation can be understood when looking at the sets of configurations used in the calculations. An open d-shell (with more than two electrons and less than two free holes) offers a considerably larger number of levels such that for the LR calculations only a limited number of configurations have been included. In fact, enough configurations have been included to predict important spectral features as observed in experiment [13], but for predicting the total radiated power

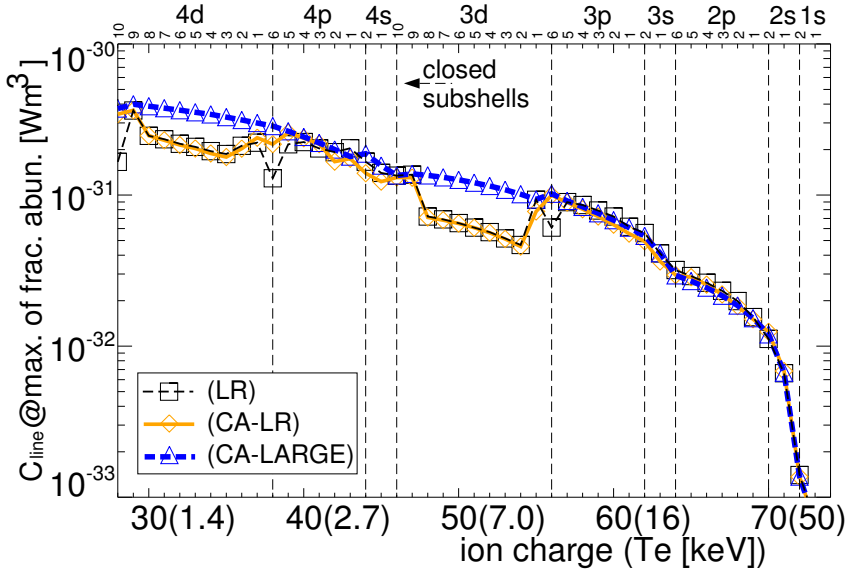

Figure 2. (colored in online-version) Line radiation rate coefficients C_{line} arising from different calculation procedures for the ionization states from Ag-like W^{28+} through He-like W^{72+}. The C_{line} is evaluated at the temperature (given in brackets for a few charge states) at which the maximum fractional abundance of the respective ionization stage occurs.

additional emissions that are not so obvious in the spectra become important. The fact that the CA-LR calculation agrees with the LR calculation supports the finding that the CA-LR calculation is consistent and numerically stable. The inclusion of further configurations in the CA-LARGE case leading to a higher cooling factor is also consistent. This means that for the determination of the cooling factor the CA-LARGE results should be used. For the cases with only one electron or free hole in an open subshell larger sets of configurations could be used in the LR case and the differences between the calculations disappear. The explanation for the second observation is not so straight forward because the discrepancies between the calculations using the same set of configurations hints towards a deficiency of the calculation method. This deficiency is there for the ionization stages Ag-like W^{28+} ($4d^{10}$), Kr-like W^{38+} ($4p^6$) and Ar-like W^{56+} ($3p^6$) with a ground state exhibiting a closed subshell denoted in brackets. However, the ground states of the ionization stages Zn-like W^{44+} ($4s^2$), Ni-like W^{46+} ($3d^{10}$), Mg-like W^{62+} ($3s^2$), Ne-like W^{64+} ($2p^6$), Be-like $^{70+}$ ($2s^2$) and He-like W^{72+} ($1s^2$) exhibit a closed subshell, too, but do not show a discrepancy between the three calculation methods. A possible explanation to the discrepancy could be the occurence of configuration mixing, which is not considered for both CA calculations. This effect may play a special role for cases with closed subshells, when the mixing of metastables is concerned but at the same time depends on the details of wave functions. The latter property could explain why the effect is apparent only for a few cases. Since, the described effect is important for only three ionization stages it plays only a small role for the total cooling factor. The associated differences would not be visible within the line thickness of the presented cooling factor below.

2.4. Resulting Cooling Factor of Tungsten

In figure 3 all above results were included, while the line radiation was taken from the LR (thin-dashed) and the CA-LARGE (thick-dashed) calculation. The LR calculation is

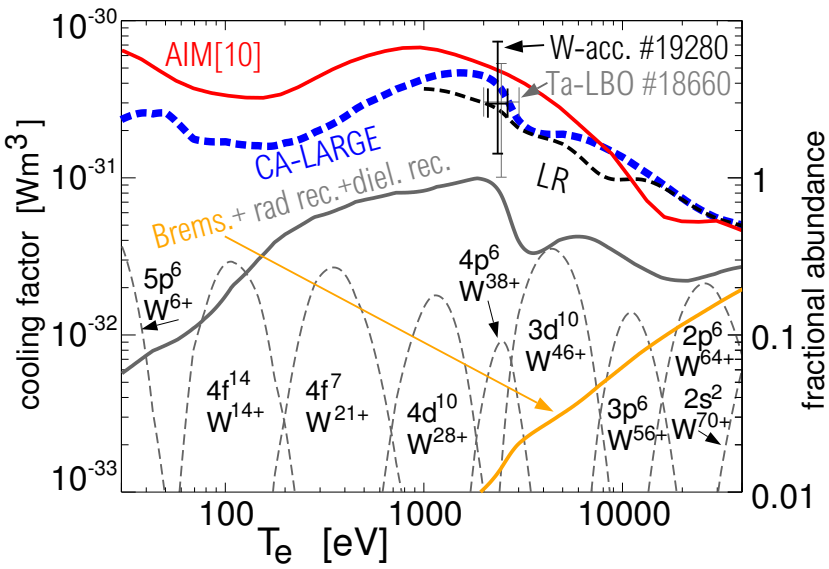

Figure 3. (colored in online-version) The total cooling factors of W from AIM [10] (red, thick, solid) and those derived from the LR (black, thin, dashed) and CA-LARGE (blue, thick, dashed) calculations are presented. The summed contributions (contained in the total cooling factors from LR and CA-LARGE) due to radiative and dielectronic recombination and by Bremsstrahlung are given as an additional curve (gray, thick, solid). The Bremsstrahlung contribution is also presented separately (orange, thick, solid). The fractional abundances are presented for a few ionization stages. The data points with error bars arise from a comparison of radiation and Bremsstrahlung as explained later in the text.

only presented above 1 keV due to the less credible data for line radiation concerning the ionization stages below Ag-like W^{28+}. The sum of the radiation emitted due to radiative and dielectronic recombination and Bremsstrahlung is presented separately to document their relative contribution, which is mostly minor. The dominant part is the line radiation for electron temperatures of up to about 20 keV. For higher electron temperatures the power from line radiation decreases, while Bremsstrahlung gets more important. Thus, its relative importance increases in this range. For comparison, the results from the average ion model are presented [10], which are in remarkably good agreement. In the range above 1 keV the differences are small and reach at most a factor of 2. In the range which is relevant for the core of a fusion reactor, i.e. for electron temperatures above 10 keV the new data gives an up to factor 1.5 higher cooling rate, which will influence moderately the limit of the maximal tolerable W concentration in a reactor, as will be shown below. Between 30 eV and 1 keV about a factor of 2 less radiation is predicted throughout. Below this temperature range the credibility of the data must be considered uncertain as the calculation of electron impact and the ionic structure data has not been optimized for the lowly charged ions. Anyhow, the cooling factor for the case of negligible transport as presented in figure 3 is not valid at the edge of a fusion plasma (approximately below a few hundred eV, depending on the device). It may be noted that the occurence of such effects and their implications on the cooling factor

have been investigated in [10]. In table 2 the values of the cooling factor L_Z, the coefficient C_{r-b}, which is the cooling factor excluding line radiation and the mean charge of the W ion are listed as a function of electron temperature. When $\log L_Z$ is linearly interpolated on the $\log T_e$ grid the resulting L_Z curve gives the calculated L_Z with deviations of less than 3% over the full T_e range of $30 - 40000$ eV.

T_e [eV]	L_Z[Wm^3]	C_{r-b}[Wm^3]	mean Z
30	2.32E-31	5.65E-33	6.77
40	2.56E-31	7.40E-33	7.95
50	2.55E-31	8.59E-33	9.13
60	2.08E-31	9.69E-33	10.25
70	1.73E-31	1.12E-32	11.46
100	1.67E-31	1.77E-32	13.47
150	1.57E-31	3.11E-32	15.70
200	1.65E-31	4.37E-32	17.71
300	1.99E-31	5.75E-32	20.18
400	2.42E-31	6.54E-32	21.62
500	2.91E-31	7.23E-32	22.81
600	3.23E-31	7.59E-32	23.75
800	3.79E-31	8.05E-32	25.33
1000	4.21E-31	8.28E-32	26.67
1500	4.59E-31	9.36E-32	30.47
2000	4.38E-31	9.76E-32	33.93
2300	3.94E-31	8.76E-32	36.08
2700	2.88E-31	5.65E-32	40.39
3000	2.28E-31	3.96E-32	42.84
3500	1.96E-31	3.32E-32	44.43
4000	1.88E-31	3.47E-32	45.30
5000	1.87E-31	4.08E-32	46.72
6000	1.79E-31	4.23E-32	48.20
7000	1.67E-31	4.09E-32	50.00
10000	1.33E-31	3.17E-32	54.58
12000	1.15E-31	2.75E-32	57.02
15000	9.47E-32	2.38E-32	59.42
20000	7.30E-32	2.22E-32	62.02
25000	6.11E-32	2.32E-32	63.64
30000	5.47E-32	2.48E-32	64.99
40000	4.95E-32	2.71E-32	66.83

Table 2. The tabulated cooling factor L_Z of W, the coefficient C_{r-b}, which denotes the cooling factor only for radiation due to recombination including Bremsstrahlung and the mean charge of the ionization equilibrium for different electron temperatures.

2.5. Sensitivity of Cooling Factor on Recombination Radiation and Rates

As for the recombination rates ad-hoc adjustments have been made, their impact on the total cooling factor is investigated with special care. Related to these adjustments are also the radiation rates due to recombination which have been connected rigidly to the recombination

rates (cf. section 2.2). In figure 4(a) the radiation due to recombination is calculated using different $f_{rec-rad}$ (cf. section 2.2), i.e. $f_{rec-rad} = 1$ and $f_{rec-rad} = 2$ instead of $f_{rec-rad} = 1.2$. These two cooling factors (thin lines) are compared to the original cooling factor (thick, dashed). The differences are small compared to the variation in $f_{rec-rad}$ by a factor of 2, demonstrating the inferior importance of the recombination radiation for the total cooling factor. In figure 4(b) the variations of the cooling factor due to a different ionization equilibrium is presented as a thin curve, while the original cooling factor is included as the thick dashed curve. The alternative ionization equilibrium is obtained by using the original

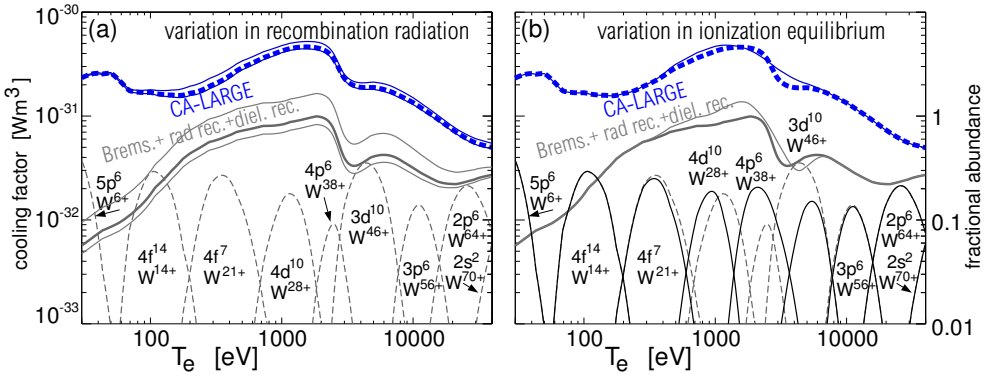

Figure 4. (colored in online-version) Similar to figure 3. (a) The cooling factor of W from CA-LARGE scheme (blue, thick, dashed) is compared to cooling factors using the assumption $f_{rec-rad} = 1$ and $f_{rec-rad} = 2$ instead of $f_{rec-rad} = 1.2$ (cf. section 2.2) (b) The cooling factor of W from CA-LARGE scheme (blue, thick, dashed) is compared to a cooling factor for which only the ionization equilibrium is differently evaluated using the original recombination rates from the average ion model (blue, thin, dashed). The alternative curves for the radiation from recombination and the abundances of ionization stages are shown in thin lines.

recombination rates from the average ion model without adjustments. The differences in the cooling factor are visible, however, the absolute value is not strongly changed. Structures in the cooling factor curve are smoothed, but there is the tendency that radiative power from one ionization stage is replaced by a similar amount from a neighboring ionization stage. Both investigations exhibit that the calculation of the line radiation is crucial for determining the cooling factor, while the accuracy of the other atomic data has relatively low impact. It should be noted that this is only true for the cooling factor while for spectral investigations the ionization equilibrium has a more profound influence.

3. Experimental Data

3.1. Observation of Spectral Features

The atomic data used to calculate the cooling factor of W have the advantage over the data from the average ion model that predictions on spectral signatures can be derived and compared to the experimentally measured ones. This has already been done in [13] where good agreement has been found for this comparison. This comparison was done after adjusting the ionization equilibrium by corrections of the recombination rates such that the experimental evidence was matched for cirumstances which allowed to ignore impurity transport. The comparisons of synthetic and measured spectra revealed that in the spectral

regions, which contain most of the radiated power, the agreement between modelled and measured emissions is better than a factor of 2 (in VUV) and a factor of 1.5 (in soft X-ray) for electron temperatures of 1-2 keV and 2-5keV, respectively. The uncertainty of the benchmark is dominated by calibration uncertainties of the VUV and soft X-ray spectrometers. The VUV spectrometer was calibrated via two methods which agreed within the uncertainties. The first method relies on modelling the carbon and boron densities which have been deduced by charge exchange recombination spectroscopy using spectral lines in the visible spectral range, which is emitted after the recombination of completely stripped ions interacting with the neutral hydrogen atoms from the neutral beam heating. Such a modelling allows for predicting the H-like and He-like emissions for both elements between 3.3 nm and 6.1 nm. Addtitionally, a cross calibration with the SPRED spectrometer was performed at 24.3 nm. The latter is an overview spectrometer which has been calibrated via branching ratios to a spectral line observed with visible spectroscopy. Both calibrations have been connected with a typical detector sensitivity curve. The procedure is described in more detail in [21]. The soft X-ray spectrometer was calibrated on the one hand by modelling the emissions of H-like and He-like Ar from 0.37 nm and 0.4 nm and on the other hand by using a large area X-ray source. Emissions for different anodes (Sn (L_α0.36 nm),Y (L_α0.64 nm), Al (K_α0.83 nm) have been quantified in lab measurements using a semiconductor detector and pulse height analysis, similar to the procedure described in [22]. Detailed EBIT measurements are available in the VUV [23, 24, 25] and in the soft X-ray range [26, 27, 28], which allow for an unambiguous line identification and benchmark for the atomic data (e.g. [20, 13]). The spectral structure of the emissions supports this good agreement, as within the spectral ranges 0.4-0.8 nm, 4-7 nm and 11-14 nm the distribution of spectral lines from experiments is reproduced by the modelling [13]. However, for few single spectral lines larger deviations could be observed (e.g Ni-like W^{46+} E2-line at 0.793 nm), which are largely understood after comparing to more detailed calculations on single ionization states. For more details on these comparisons see [13, 29, 30].

Electron temperatures above 5 keV are not easily accessible in todays fusion experiments, but respective spectral lines can be studied in EBIT experiments. Measurements performed at EBITs in the EUV range [31, 32] are consistent with the calculations in terms of dominant spectral lines and detailed benchmarks with the data from the Berlin EBIT in the soft X-ray range yield good agreement [33, 34]. It has been found in [33, 34], that the important spectral features are reproduced by the LR calculations predicting most of the spectral lines within an accuracy of factor of 2, while only a few special spectral lines exhibited larger discrepancies. This yields the same accuracy as found for the tokamak spectra in the range of 0.4-0.8 nm. Taking these results the obtained atomic data exhibit a high credibility. On the other hand, the agreement with the data from AIM calculations [9, 10] validates these older results.

3.2. Direct Measurement of the Cooling Factor

A direct measurement of the cooling factor in a plasma relies on the absolute determination of the W density independent from the total radiation measurement. In principle, a small change of the W concentration leads to an increase in the effective ion charge $Z_{eff} = \frac{\Sigma_k n_k Z_k^2}{\Sigma_k n_k Z_k}$ (where n_k and Z_k are the density and charge of the various ion species) which is diagnosed via the Bremsstrahlung intensity. Consequently, the direct measurement of the cooling factor relies on determining a small change of Z_{eff} due to an increased W concentration and comparing this to the change in radiated power. It is tedious to perform such experiments in a fusion plasma, because a large radiation increase means troublesome operation of the plasma. At

ASDEX Upgrade the best experimental data for such an experiment was obtained for a Ta (Z=73) injection by laser blow-off. The data point is introduced in figure 3 (gray, thin), because the differences of the cooling factor of Ta and W are expected to be small compared to the uncertainties (cf. [21]). In the following a slightly different approach, which makes use of a peculiar behaviour of a plasma dicharge is explained in detail.

At ASDEX Upgrade there are eight different heating beams available, which all inject neutral deuterium into a magnetically confined fusion plasma. The beams inject continuously the neutrals with energies up to 93 keV, such that they penetrate the plasma. The heating of the plasma is performed after the neutrals are ionized and confined by the magnetic field. The heating location is defined by the injection geometry and in detail also by plasma parameters. In figure 5, the geometry of two beams are depicted, one heating the center of a discharge and one pointing away from the center. Additionally, the geometry of a few plasma diagnostics are presented, which are discussed below .

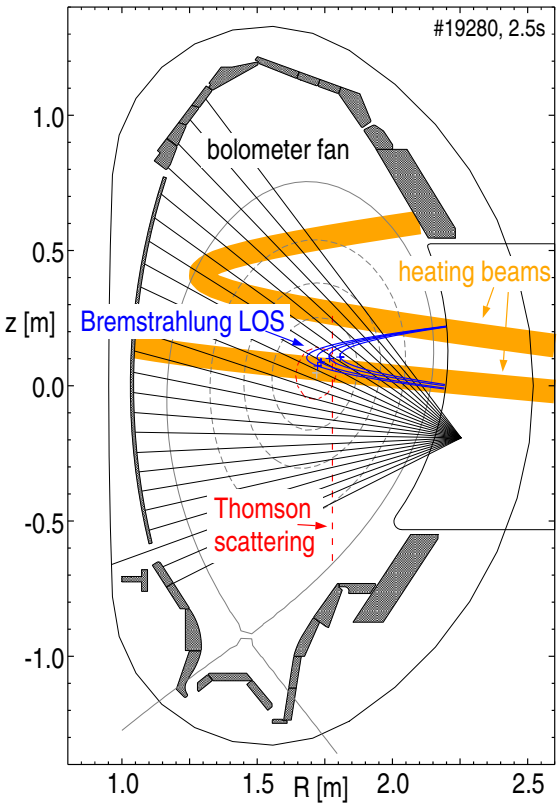

Figure 5. (colored in online-version) Geometry of heating beams, lines of sight of the bolometer and Bremsstrahlung measurement and Thomson scattering along with the plasma equilibrium of discharge #19280 at 2.5 s. The curved trajectories result from the projection of tangential LOS and beam lines in the poloidal plane.

In the discharge #19280, the plasma is heated with these neutral deuterium beams. Each of the eight beams is turned on for 500 ms in sequence. The beam which is switched on at 2.0 s is aligned such that the innermost 10-20 cm of the plasma core are not heated, which leads to a small turbulent transport in that region. This decrease in turbulent transport makes

the neoclassical transport, i.e. transport based on particle trajectories and collisions, dominant [35, 36]. In detail, the neoclassical inward pinch is acting on all impurity species, while its strength is approximately proportional to the charge of the species. This inward drift relies on a gradient of the background deuterium ion density and can be mitigated or reversed by an ion temperature gradient, which is not the case in the actual discharge. The inward pinch leads to so-called impurity accumulation which is dominated by W as can be deduced from the impurity mix available at ASDEX Upgrade. At 2.5 s another beam is turned on heating the plasma core which starts reversing impurity accumulation by increasing the turbulent transport. Figure 6 (a) depicts the radiation profiles derived from the measurements of the

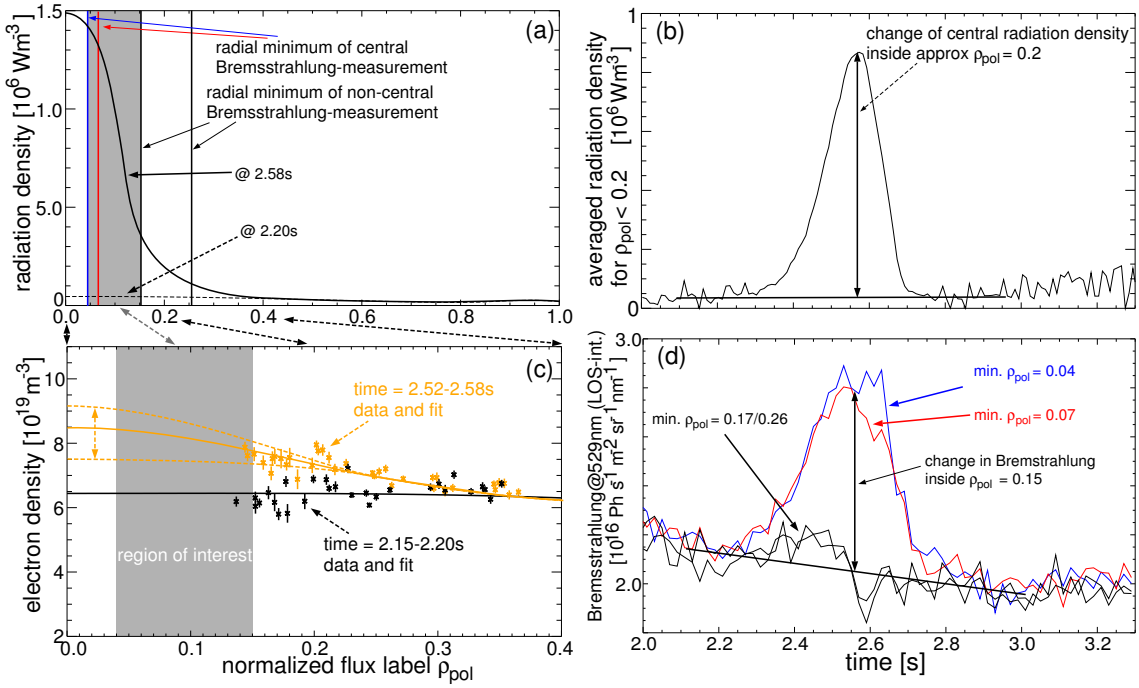

Figure 6. (colored in online-version) (a) Deconvoluted radiation profile before and during W-accumulation. Vertical lines denote the minimum radius seen by four lines of sight measuring Bremsstrahlung. (b) Evolution of the radiation density averaged within $0 < \rho_{pol} < 0.2$. (c) Electron density measurement (Thomson scattering) and respective fits before and during W-accumulation. (d) Evolution of four (cf. part (a) of this figure) LOS-integrated Bremsstrahlung measurements.

bolometer fan as depicted in figure 5 before and during the accumulation phase and figure 6 (b) documents the evolution of the radiated power density averaged inside $\rho_{pol} < 0.2$, i.e. the core region of the plasma with a radius of approximately 7-10 cm. In figure 6 (d) the Bremsstrahlung measurement integrated along a line of sight (LOS) with a toroidal viewing geometry (cf. figure 5) are presented. An increase in Bremsstrahlung is only seen for lines of sight (LOS) which integrate over plasma radiation inside $\rho_{pol} < 0.15$. A detailed analysis was performed using the fits to the measured electron densities depicted in 6 (c). The uncertainty of the fit is relatively large because the measurement does not fully cover the core region. However, the shaded region is only about 4 cm wide and the electron density profile cannot change arbitrarily in this region due to constraints from plasma transport considerations. The

fit is a spline fucntion, which is forced to have a zero derivative in the plasma center. The obtained variation in the electron density fit is indicated with the dashed lines. For stronger variations of the electron densities the uncertainties for the cooling factor would increase. The result of this analysis is introduced as a data point in figure 3 (black, thin). As can be seen the value and the error bars are comparable to those from the Ta experiment and both measurements are in agreement with all theoretical curves. It must be noted that some uncertainties have not been included in the error bars of the W-data point. For instance, it is assumed that the change of Z_{eff} is exclusivly caused by W and that the contribution of other ions to the Z_{eff} of 2.1 ± 0.1 does not vary during the accumulation phase. Therefore, the measurement must be interpreted with care and the main conlusion of the analysis is that the cooling factor is consistent with observations within less than an order of magnitude.

4. Implications on Operation of a Fusion Reactor

The newly obtained cooling factor is used to assess the influence of W as an impurity in a future reactor on the condition for the thermonuclear burn. The ignition condition is derived from the heating of the plasma by α-particles from DT-fusion, which must compensate the energy losses of the plasma due to transport and radiation. For this balance the energy confinement time τ_E is used to describe the losses by transport, while radiation losses are treated using the cooling factor as obtained in this work. Helium is included in the condition as it is naturally produced by the fusion process and then dilutes the fuel. To describe the fact that He is less efficiently pumped from the plasma than the fuel, a He confinement time $\tau_{He} = 5\tau_E$ is used which reflects the predictions in [37]. For the different values of temperatures T the ignition will occur at different values of $nT\tau_E$, where n is the density. The additional impurities alter the conditions for ignition and might lead to the disappearence of a ignition condition for all T due to dilution and radiation. For W the effect of radiation is much more important than the dilution due to the large cooling factor. For more details of the evaluation of the ignition curves, confer to [38]. The scheme used in the present work corresponds to case 4 in section 3 of [38]. In [3] the evaluation of the burn condition has been performed in the same manner, but with the data from the AIM. In figure 7(a), the curves are shown

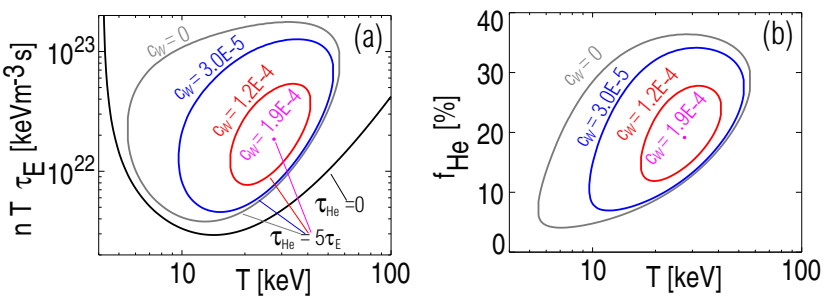

Figure 7. (colored in online-version) (a) Ignition curves in the presence of different W concentrations for the case that $\tau_{He} = 5\tau_E$ along with the curve for no He and no W for reference. (b) Equilibrium He concentrations corresponding to burn curves from part (a).

which represent conditions for which ignition appears. The curve without He is presented for reference only and will not be discussed below. For the curves with He, the corresponding He concentration curves are presented in figure 7(b). For a W concentration of $3.0 \cdot 10^{-5}$, the minimum $nT\tau_E$ is 20% larger than the value for no W, which is $3.8 \cdot 10^{21}$ keV m^{-3} s and its

minimum is found at $T = 15.2$ keV, instead of $T = 12.8$ keV for the case without W. The respective He-concentrations are approximately 8% and 6%. When comparing these values to the results using the AIM data, the corresponding change of $nT\tau_E$ by 20% is observed for a W concentration of $4.5 \cdot 10^{-5}$, as the cooling factor based on the AIM data is lower in the respective temperature range. The burn condition is not anymore achievable for W concentrations above $1.9 \cdot 10^{-4}$ using the new cooling factor, while the cooling factor from the AIM calculation gives an upper limit of $2.3 \cdot 10^{-4}$. However, it should be noted that in a reactor other impurities will be abundant additionally to W which implies that a realistic limit for the maximum W concentration is in the range of several 10^{-5}.

5. Summary

This work follows up work [13] on the modelling of dominant spectral features in the W spectrum. In the course of this earlier work the ionization equilibrium was matched to experiment in the electron temperature range 1-5 keV by adjustments of the recombination rates. These findings were used in the actual work to calculate the cooling factor of W. The line radiation has been evaluated by calculations on atomic/ionic structures and excitation rates using the plane-wave Born approximation. All calculations have been performed with the Cowan code using the infrastructure and collisional-radiative modelling of the ADAS project. Level-resolved calculations have been compared to less elaborate configuration averaged calculations in order to extend the involved number of configurations entering the calculations and also to extend the calculations to ions with a lower charge than Ag-like W^{28+}. The results of the different calculation approaches could be understood qualitativly and the best suited data to enter the cooling factor originated from the configuration averaged calculation with a very large set of input configurations. The total radiated power predicted by level-resolved calculations, which reproduce the dominant spectral features observed in experiment, is matched within a few percent by the configuration averaged calculation scheme using the same set of input configurations. For a few exceptions, i.e. three ionization states with closed subshells, differences between the two calculation methods as large as 50% in line radiation are observed, but play only an insignificant role for the total cooling factor. The radiated power during recombination (i.e. radiative and dielectronic recombination) is predicted by taking the recombination rate and assuming that 1.2 times the ionization potential is radiated in the course of recombination. This approach is chosen, to obtain data consistent to the recombination rates which have been adjusted to experimental observations. However, details of the recombination radiation are not important since line radiation is the dominant radiation source for the plasma parameters considered here. A study was performed to ensure that uncertainties in the recombination rates and the connected radiation have only minor influence on the cooling factor. Additionally, the Bremsstrahlung is taken into account. The resulting cooling factor is given in tabulated form. Its value at approx. 2.3 keV is measured in experiment by comparing the total radiation to the Bremsstrahlung during a special phase of a plasma discharge in ASDEX Upgrade. The measurement agrees with the calculation, however, the uncertainties of the measurement are nearly one order of magnitude. When comparing the actual cooling factor to that derived from the average ion model (AIM), about a factor of 2 less radiation is predicted below 1 keV, while the differences decrease for higher electron temperatures. Both cooling factors are quite similar above 6 keV, while the newly evaluated cooling factor slightly exceeds the cooling factor from the AIM above electron temperatures of approx. 10 keV. Therefore, the predictions of the maximum tolerable tungsten concentration for a fusion reactor, which prior to this work were based on the AIM, are reduced only slightly by about 20-35%.

References

[1] N. Noda, V. Philipps, and R. Neu, Journal of Nuclear Materials **241–243**, 227 (1997).
[2] R. Neu, Physica Scripta **T123**, 33 (2006).
[3] R. Neu *et al.*, Fusion Engineering and Design **65**, 367 (2003).
[4] R. Isler, R. Neidigh, and R. Cowan, Phys. Lett. **A63**, 295 (1977).
[5] E. Hinnov and M. Mattioli, Phys. Lett. **A66**, 109 (1978).
[6] R. Neu *et al.*, Nuclear Fusion **45**, 209 (2005).
[7] R. Neu *et al.*, Plasma Physics and Controlled Fusion **49**, B59 (2007).
[8] A. C. C. Sips and O. Gruber, for the ASDEX Upgrade Team, Plasma Physics and Controlled Fusion **50**, 124028 (2008).
[9] D. Post *et al.*, At. Data Nucl. Data Tables **20**, 397 (1977).
[10] D. Post, J. Abdallah, R. Clark, and N. Putvinskaya, Phys. Plasmas **2**, 2328 (1995).
[11] R. D. Cowan, *The Theory of Atomic Structure and Spectra (Los Alamos Series in Basic and Applied Sciences)* (University of California Press, California, 1981).
[12] A. Foster, doctoral thesis at Department of Physics, 'On the Behaviour and Radiating Properties of Heavy Elements in Fusion Plasmas', University of Strathclyde, Glasgow, UK (2008) - http://adas.phys.strath.ac.uk/theses/foster_thesis.pdf
[13] T. Pütterich *et al.*, Plasma Physics and Controlled Fusion **50**, 085016 (2008).
[14] S. D. Loch *et al.*, Physical Review A (Atomic, Molecular, and Optical Physics) **72**, 052716 (2005).
[15] E. Behar, R. Doron, P. Mandelbaum, and J. L. Schwob, Phys. Rev. A **58**, 2115 (1998).
[16] A. Peleg, E. Behar, P. Mandelbaum, and J. L. Schwob, Phys. Rev. A **57**, 3493 (1998).
[17] E. Behar, P. Mandelbaum, and J. L. Schwob, Phys. Rev. A **59**, 2787 (1999).
[18] W. J. Karzas and R. Latter, Astrophysical Journal — Supplement Series **6**, 167 (1961).
[19] H. P. Summers, The ADAS User Manual, version 2.6 http://adas.phys.strath.ac.uk (2004).
[20] T. Pütterich *et al.*, J. Phys. B: At. Mol. Opt. Phys. **38**, 3071 (2005).
[21] T. Pütterich, Technical Report No. 10/29, IPP Garching, Germany, 2006, doctoral thesis at Universität Augsburg ,'Investigations on Spectroscopic Diagnostic of High-Z Elements in Fusion Plasmas'
[22] R. Neu *et al.*, Review of Scientific Instruments **67**, 1829 (1996).
[23] R. Radtke *et al.*, Phys. Rev. A **64**, 012720 (2001).
[24] Y. Ralchenko *et al.*, Journal of Physics B: Atomic, Molecular and Optical Physics **40**, 3861 (2007).
[25] S. B. Utter, P. Beiersdorfer, and E. Träbert, Can. J. Phys. **80**, 1503 (2002).
[26] R. Radtke, C. Biedermann, P. Mandelbaum, and J. L. Schwob, in *HCI 2006: 13th International Conference on the Physics of Highly Charged Ions*, Vol. 58 of *J. Phys. Conf. Ser.*, edited by R. McCullough *et al.* (IOP, Bristol , England, 2007), pp. 113–116.
[27] P. Neill *et al.*, Can. J. Phys. **82**, 931 (2004).
[28] Y. Ralchenko *et al.*, Physical Review A (Atomic, Molecular, and Optical Physics) **74**, 042514 (2006).
[29] C. P. Ballance and D. C. Griffin, Journal of Physics B: Atomic, Molecular and Optical Physics **39**, 3617 (2006).
[30] Y. Ralchenko, Journal of Physics B: Atomic, Molecular and Optical Physics **40**, F175 (2007).
[31] Y. Ralchenko *et al.*, J. Phys. B-At. Mol. Opt. Phys. **41**, 021003 (2008).
[32] U. Feldman, J. E. Seely, E. Landi, and Y. Ralchenko, Nucl. Fusion **48**, 045004 (2008).
[33] C. Biedermann, R. Radtke, R. Seidel, and T. Pütterich, Physica Scripta **T134**, 014026 (2009).
[34] R. Neu *et al.*, in *Highly Charged Ions*, edited by R. Hutton *et al.* (CRC Press, London, England, 2010), to be published.
[35] R. Dux *et al.*, Plasma Physics and Controlled Fusion **45**, 1815 (2003).
[36] R. Dux, Fusion Science and Technology **44**, 708 (2003).
[37] D. Campbell, Phys. Plasm. **8**, 2041 (2000).
[38] D. Reiter, G. H. Wolf, and H. Kever, Nuclear Fusion **30**, 2141 (1990).